Fully integrated workflow for scalable and cost-effective manufacturing of high-quality AR waveguides

Brian Bilenberg[1], Ankit Bisht[1], Vladimir Miljkovic[1], Frederik Bachhuber[2], Christian Hellmann[3], Leo Peltomaa[4], Murat Deveci[5], Brian Szychowski[6], Aleksandr Razumtcev[6], Neil Pschirer[6], René Liebers[7], Rana Al-Amidi[8], Erhan Ercan[8], Mariana Ballottin[8]
NIL Technology ApS (Denmark)[1]; SCHOTT AG (Germany)[2]; LightTrans International GmbH (Germany)[3]; OptoFidelity Oy (Finland)[4]; OptoFidelity Inc. (United States)[5]; Pixelligent Technologies LLC (United States)[6]; 3D-Micromac AG (Germany)[7]; Morphotonics B.V. (Netherlands)[8]

ABSTRACT

Scalable and cost-effective production of optical waveguides remains a cornerstone for Augmented Reality (AR) glasses. In this work, a diffractive waveguide design featuring multi-depth slanted gratings with a 25° slant angle is used to validate key components of a fully automated large-area Roll-to-Plate (R2P) nanoimprint lithography line. Inkjet printing is used to locally dispense a high refractive index (HRI, n = 1.8) resin across ultra-flat square HRI glass wafers (n = 2.0), an important capability not possible with spin coating. Carrier-based aligned imprinting is performed using a new tool capable of consistent performance across multiple runs per stamp. A modular laser singulation system enables precise, defect-free separation of individual lenses. Optical quality is assessed through high-resolution MTF measurements, automated visual inspection, and simulation, allowing correlation of process parameters and defects with waveguide performance. This work demonstrates a fully integrated path to scalable manufacturing of high-quality next-generation AR optics.

Keywords: augmented reality, waveguides, high refractive index materials, large-area nanoimprint lithography (NIL), optical design, metrology, automated singulation, optical simulation.

1. INTRODUCTION

The widespread adoption of Augmented Reality (AR) glasses depends not only on advances in optical design and system integration, but also on the availability of manufacturing technologies capable of delivering high-quality waveguides at scale and at acceptable cost. Over the past decade, significant progress has been made in diffractive waveguide architectures, materials, and optical performance. However, translating these designs into high-volume production remains challenging due to the tight tolerances required for grating fidelity, residual layer thickness control, and substrate flatness, particularly when high refractive index materials and complex, multi-depth grating structures are involved.

Conventional wafer-level fabrication approaches provide high pattern fidelity but are often limited in throughput and material utilization, while large-area manufacturing techniques can struggle to maintain the uniformity and overlay precision required for advanced AR waveguides. As a result, there is an increasing interest in integrated manufacturing workflows that combine precision nano-fabrication with scalable, automated processing. Such workflows must accommodate diverse substrate geometries, advanced materials, and downstream processes including singulation and metrology, while preserving optical performance across large production volumes.

Within this context, we have been exploring fully integrated manufacturing solutions that span waveguide design, master fabrication, substrate development, materials engineering, large-area nanoimprinting, singulation, and optical metrology. This paper presents a collaborative demonstration of such a workflow, centered on large-area Roll-to-Plate (R2P) nanoimprinting combined with inkjet-based material deposition, advanced glass substrates, high-refractive-index resins, and automated downstream processing. By validating each step within a coordinated manufacturing chain, this work aims to demonstrate a practical and scalable path towards cost-effective, high-quality AR waveguide production suitable for next-generation AR eyewear.

2. KEY TECHNOLOGIES

2.1 Waveguide design & simulation (LightTrans)

The waveguide design developed in the previous year [5], featuring multi-depth slanted gratings with a 25° slant angle, served as a demanding optical test vehicle to validate key capabilities of the automated Roll-to-Plate (R2P) nanoimprint line. To quantify the tolerance limits of the fabrication process, we performed a systematic analysis correlating realistic fabrication deviations (derived from partner-supplied metrology of fabricated samples) with simulated optical performance.

All simulations were conducted using VirtualLab Fusion, which provides advanced modeling of the complete waveguide. This approach rigorously accounts for polarization, interference, coherence, and diffraction, enabling the calculation of basic metrics (e.g., efficiency, uniformity) and advanced image-quality parameters such as the point spread function (PSF) and modulation transfer function (MTF). The latter are critical for assessing the final visual performance of AR glasses and require an accurate diffractive model.

2.2 Master (NIL Technology)

A single full eye-piece Surface Relief Grating (SRG) waveguide 6-inch master Figure 1a was fabricated previously [5] on a silicon substrate tailored to the optical design referred to in section 2.1. The gratings on the master were fabricated using electron beam lithography and structures were transferred into the substrate using proprietary dry etch processes. This approach for master fabrication ensures the highest possible quality of SRGs, with electron beam lithography providing high pitch and lateral dimensional accuracy and dry etching delivering precise control of grating depths and high structure fidelity. Figure 1c shows a stitched optical image of the master taken with a 5X objective. Second generation replica from the master (Figure 1b) acts as a working master for further replications. Etch processes are carefully calibrated on monitor chips (gratings shown in Figure 1 d – h), which served as test substrates to validate etch parameters. The structures on the monitor chips were characterized using cross sectional SEM before etching the gratings on the final master. This process allows for independent optimization of each of the 18 distinct grating sections on the master, ensuring uniformity and precision across the design to meet the stringent requirements of AR waveguide masters.

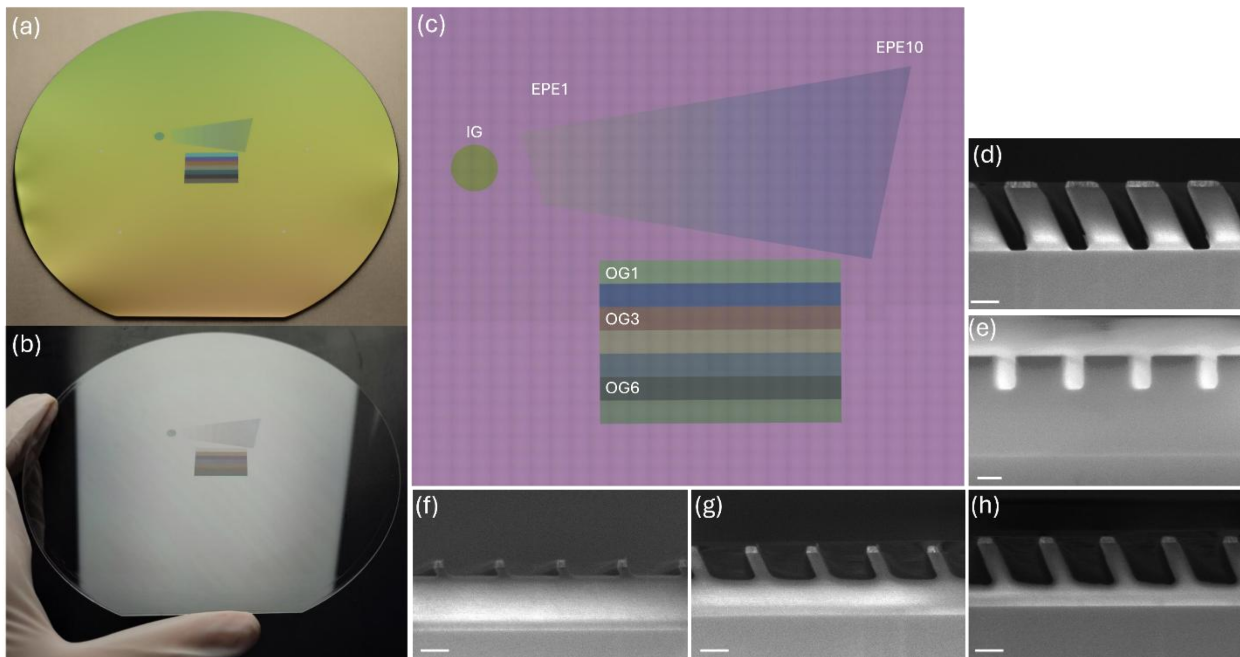

Figure 1 (a) Camera image of the 6-inch master, (b) camera image of a second generation working master produced from the master in (a), (c) stitched automated microscope images of the master taken with a 5x objective. The output grating (OC) consists of sections with

increasing depth and filling fraction from OG1 to OG7, while the expander grating (EPE) is composed of sections with increasing depth and decreasing filling fraction from EPE1 to EPE10, (d) cross-section SEM image of IC monitor chip (scale bar 200 nm), (e) representative cross-section SEM image of binary gratings corresponding to EPE10 in (c) (scale bar 100 nm), (f-h) cross sectional SEM images of OG1, OG3 and OG6, respectively. (scale bar 200 nm). In (d-h) the hard mask has not been removed.

2.3 Glass substrates (SCHOTT)

High-index optical glass remains a cornerstone for AR waveguides, where surface precision directly impacts image quality. SCHOTT's RealView® portfolio has demonstrated refractive indices of n = 2.0 and beyond, with formats up to 300 mm (round and square), available in an Ultra grade with TTV values well below 0.5 µm. For this project, SCHOTT introduces a new rectangular wafer format of 151 mm × 120 mm based on n = 2.0 glass (RealView® 2.0), maintaining the same Ultra grade specification as conventional round wafers. This format combines perfect area utilization across glass melting, polishing, and nanoimprinting, delivering significant cost benefits for large-scale manufacturing.

From a glass melting perspective, the smaller width improves meltability and yields, and it enables access to challenging glass types such as super high refractive index glasses (n > 2.1), including RealView® 2.14 presented previously at SPIE. Additionally, the rectangular format eliminates material waste from converting rectangular glass strips into round cylinders and wafers. While rectangular wafers on round-based spinning polishing tools are inherently less ideal, the chosen format of 151 mm × 120 mm minimizes this penalty. Another key advantage is that significantly more eyepieces per area can be placed on rectangular versus round wafers.

Flatness remains critical: local wedge and total thickness variation (TTV) below 0.5 µm are maintained across the active areas, ensuring minimal beam path aberrations and preserving Modulation Transfer Function (MTF). This is especially important as thinner substrates become standard for weight reduction, increasing the number of internal reflections and amplifying the need for ultraflat surfaces.

The substrates integrate seamlessly into Morphotonics' large-area Roll-to-Plate (R2P) nanoimprinting workflow. The rectangular format enables stitching of smaller panels, optimizing imprint layouts and delivering higher throughput per carrier compared to circular wafers, as illustrated in Figure 2.

Figure 2 Comparison of wafer layouts on equal-sized Gen3 carriers (620 mm × 650 mm): left shows 20 rectangular panels (5 × 4 grid, 151 mm × 120 mm), right shows 9 round wafers (3 × 3 grid, 200 mm diameter). The rectangular format more than doubles eyepiece count per imprint cycle and achieves significantly higher area utilization (~89.9% vs. ~70.2%), enabling improved throughput and reduced material waste.

By combining material innovation, optimized geometry, and manufacturing efficiency, this rectangular wafer format provides a scalable solution for next-generation AR waveguides.

2.4 High refractive index resins (Pixelligent)

UV-curable high-RI resin is a critical material for the mass production of AR waveguides. The key nanoscale diffractive optical components responsible for coupling and propagating light in a waveguide are fabricated by nano-imprinting of the resin. Pixelligent produces industry-leading nanocomposites designed to maximize the optical efficiency of AR/XR/MR waveguides by ensuring refractive index and structure uniformity, high transmittance and low haze, all while maintaining a low residual layer thickness (RLT).

Pixelligent's PixNIL® JT1 and JCS1 solvent-containing formulations were utilized for R2P waveguide production. Both formulations are designed to produce thin films with a refractive index of 1.83 at 589 nm and are equally compatible with inkjet deposition and nanoimprinting due to their low viscosity (~7 cP). Film thicknesses in the range between 50 and 450 nm can be produced while maintaining low RLT. Inkjet compatibility of both formulations allows for precise control of coating thickness and ensures large-scale replication. Both materials are compatible with a variety of NIL stamps, different grating geometries, and are compatible with commercial inkjet and NIL equipment.

The PixNIL® JT1 nanocomposite is based on proprietary PixClear® titania nanocrystals with a tight particle size distribution (Figure 3), whereas JCS1 is based on PixCor® core-shell 25 nm nanocrystals designed for improved photostability. Leveraging in-house nanocrystals with precisely controlled shape, size, and surface chemistry enables Pixelligent to produce formulations with superior optical properties, such as image uniformity, clarity, and low scattering.

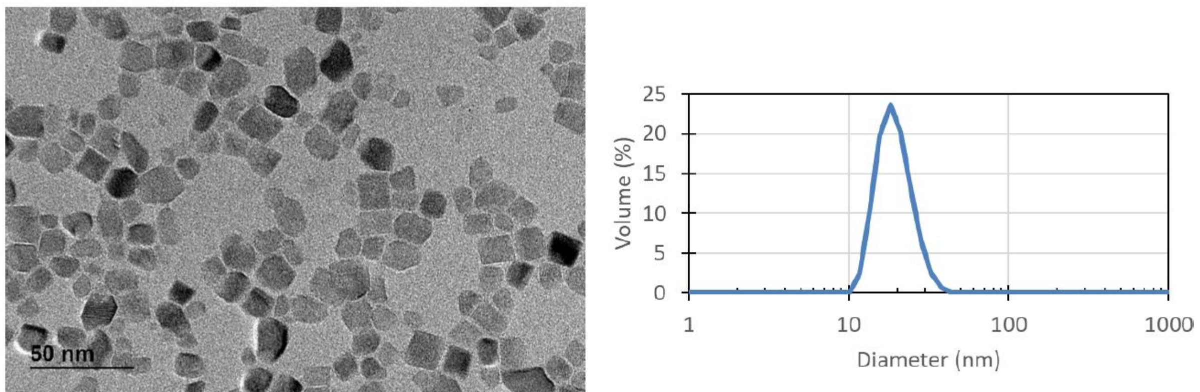

Figure 3 Left – TEM image of Pixelligent's titania nanocrystals. Right – Typical DLS result for the nanocrystals showcasing tight size distribution.

2.5 Large-Area Nanoimprinting (Morphotonics)

Morphotonics' large-area roll-to-plate (R2P) NIL technology enables high-throughput manufacturing while maintaining excellent replication quality and scalability. Results presented by this consortium of companies in the previous years of SPIE AR|VR|XR conferences [1-3, 5] demonstrated the technology's ability to accurately replicate surface-relief gratings (SRGs) such as blazed, slanted and binary while preserving fine replication details and maintaining consistent pitch uniformity.

In this work, we advance the process further by integrating inkjet printing with large-area nanoimprint lithography (NIL). This combined approach enables the production of the intricate features required for high-performance AR waveguides while maintaining the accuracy needed for large-scale manufacturing. Large-area NIL complements this by delivering highly accurate replication of these features across extensive surfaces at high throughput. As a result, uniformity and replication fidelity are maintained even as the imprint area increases, an important factor for reliable, large-scale production.

The AR waveguides were replicated from an upscaled working master into high refractive index material using the Morphotonics Portis line. The Portis P1100 is used for the primer to promote adhesion of the UV curable resins, and the Portis NIL1100 for the nanoimprint of the textures. The schematic in Figure 4 presents the cycle process used to produce the waveguides, which includes: a) surface treatment of the glass substrate using Portis P1100 to promote inkjet resin adhesion, b) dispense inkjet resin on the rectangular substrate, and c) replication of the AR slanted-grating texture using a

flex stamp carrying inverted texture in Portis NIL1100. The flexible stamp used in this work contained nine areas, each of these areas was composed of the upscaled texture of 4 waveguides.

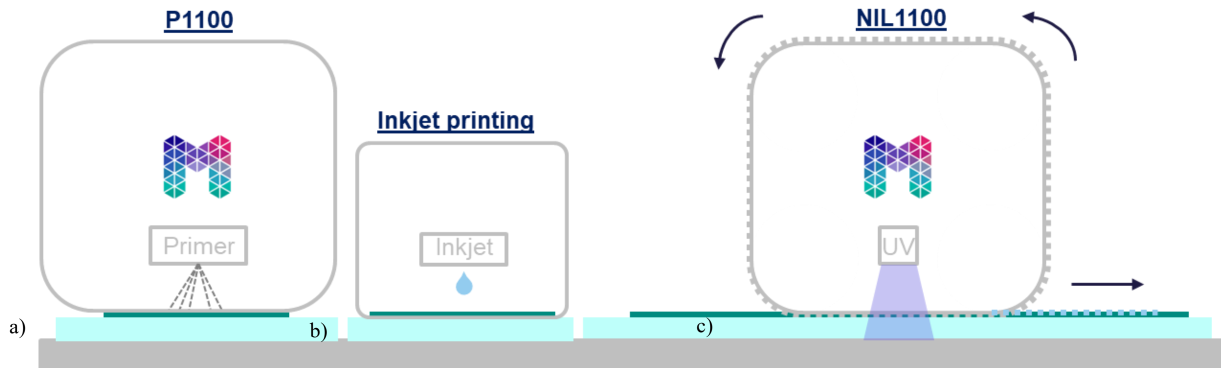

Figure 4 Schematic of cycle process: a) prime the substrate by using Portis P1100, b) dispense inkjet resin by using inkjet printing, and c) replicate the texture using Portis NIL1100.

The Roll-to-Plate (R2P) nanoimprint lithography machines of Morphotonics can imprint multiple smaller substrates at once using a wafer carrier, which is a plate with pockets that hold each substrate in place and create a smooth, even surface for imprinting. This approach is beneficial for the manufacturing AR waveguides, where high-refractive-index materials are costly and uniform patterning is essential.

Morphotonics' nanoimprint technology can be integrated into existing wafer-based manufacturing processes. In earlier work, five 200 mm high-refractive-index wafers were successfully imprinted simultaneously using a Gen3 wafer carrier (550 mm × 650 mm) by using jet technology and spin coating [5]. To further demonstrate scalability and compatibility with rectangular wafers, nine high-refractive-index wafers (120 mm × 151 mm × 1 mm) were imprinted at once using an enlarged Gen3 wafer carrier (620 mm × 650 mm). Eleven imprint cycles were performed with the same flexible stamp to confirm that both uniformity and high imprint quality were consistently maintained across all substrates when using inkjet printing.

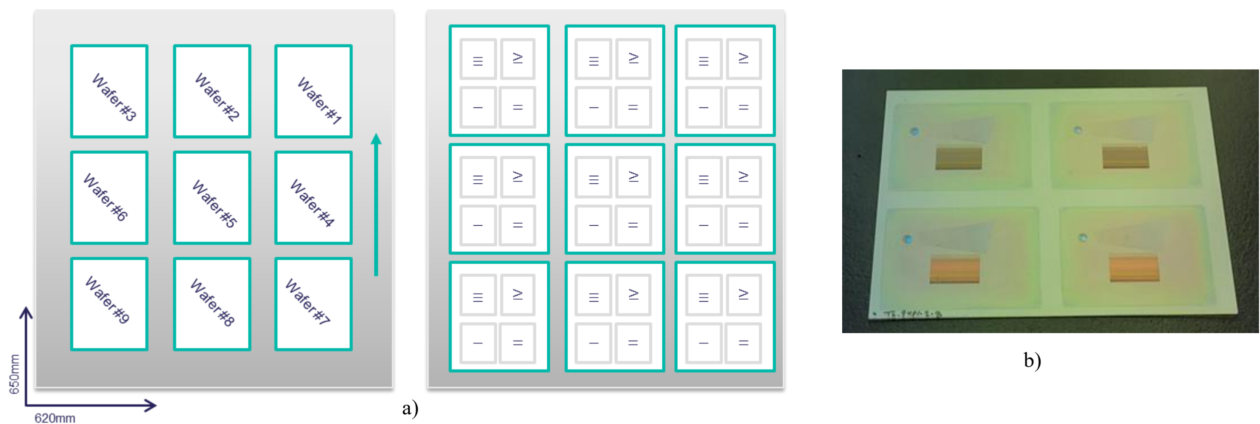

Figure 5 Schematic of the imprint layout 620 mm x 650 mm for nine wafers rectangular substrates of 151 mm x 120 mm x 1 mm with four AR waveguides per wafer; labeled by wafer (1–9) and waveguide (I–IV) positions. b) Resulting imprinted wafer showing four AR waveguides produced using a resin with refractive index 1.83 on 2.0 refractive index SCHOTT Real View 2.0 ®glass rectangular substrates.

On each 120 mm × 151 mm × 1 mm rectangular wafer, four slanted AR waveguides (**Error! Reference source not found.** and Figure) were replicated, as illustrated in Figure 5. Across 11 imprint cycles, a total of 396 AR waveguides were

produced. The first ten cycles were replicated using the high-refractive-index (HRI) material PixNIL® JT1 (n = 1.83), while the remaining cycle was replicated using PixNIL® JCS1. All cycles were done using 2.0 refractive index SCHOTT Real View 2.0 ® glass rectangular substrates.

Inkjet printing is an effective method of dispensing resins for the replication of AR waveguides with high precision and material efficiency. By providing precise control over resin volume and placement, this approach ensures uniformity, high-quality replication, enabling the scalable production of cost-effective, high-performance diffractive waveguides. The wafer-based imprinting method demonstrated in this work will be applied in the Cypris X600 platform, a fully automated, modular system for the replication of AR waveguides that integrates Roll-to-Plate (R2P) nanoimprint lithography with high-resolution inkjet printing [6]. This combination will enable precise pattern replication, accurate resin deposition, and high-throughput processing, making it ideally suited for scalable and cost-effective manufacturing of AR waveguides with uniform quality and high optical performance.

2.6 Waveguide singulation (3D-Micromac)

3D-Micromac optimized its laser cutting process specifically for high refractive index substrates used to produce AR eyepieces, ensuring high yield and precision. The equipment used is based on laser modification cutting, a recognized production process in the display industry known for its ability to produce high-quality cuts with minimal edge defects. The process flow of this cutting process is a 2 step process. First, the glass (filamentation) is modified along a pre-determined curve (the intended break line) and through the entire material thickness using pico- or femtosecond laser pulses. Each point of modification is created by the local impact of a single laser pulse or pulse bursts. Then, a secondary process step is required to separate the glass along the break line. For the applied free-form geometries, the required stress is typically introduced by exposing the modification and its surrounding material to a CO_2 laser.

Within the current framework of the joint AR Consortium project for manufacturing waveguides for augmented-reality eyewear, the presented system focuses on the high-precision singulation of high index-glass wafers whether round or square shaped into individual eyepieces. The overarching objective is to achieve maximum yield while ensuring outstanding cut-edge quality, thereby enabling industrial-scale production of eyepieces with minimal defects.

Building on the established microPOLAR machine platform (Figure 6), the latest system generation introduces several key enhancements aimed at supporting both research-driven process development and the transition toward high-volume manufacturing. As customer requirements increasingly demand high flexibility and maximum transferability of process parameters from R&D environments to mass-production scenarios, the platform has been extended with a R&D focused machine variant while maintaining scalable system performance. This shift enables users to iterate processes more effectively and to stabilize critical parameters before transitioning into ramp-up phases.

A key aspect of the redesign is the introduction of a more modular workflow architecture. Compared to fully integrated and tightly chained process sequences, the new configuration incorporates a higher number of individually deployable process modules. This structure increases robustness during production ramp-up, simplifies intervention during process optimization, and enables improved in-field serviceability.

Material flow has also been significantly improved. Intermediate buffering between process steps is now easily achievable, supporting higher operational stability and reducing the risk of bottlenecks. In addition, the system has been optimized for processing rectangular wafer geometries, extending its applicability to new substrate formats.

Another major enhancement concerns the optional integration of wafer carriers. The system can now adapt to advanced carrier-handling concepts that improve throughput, process stability, and waste-management efficiency. Carrier handling not only accelerates the overall workflow but also contributes to more reliable wafer fixation and transport throughout the singulation process. In addition, we can now guarantee significantly simpler interlinking with the neighboring Morphotonics machines that implement the nanoimprint process step. The throughputs and the interfaces of the two systems are optimally coordinated with each other.

Through these developments, system complexity has been reduced while operational stability has been increased. Depending on system configuration, the achievable throughput now reaches up to 3 million eyepieces per tool when using 2 wafer carrier, and approximately 2.4 million eyepieces per tool with one wafer on carrier (Figure 6).

Figure 6 Left: MicroPOLAR machine including SEMI Compliant wafer loadports and customized eyepiece to tray handling unit, Right: High Index-Glas Wafer (diameter 200 mm) on carrier with pre-singulated Eyepieces

2.7 Metrology (OptoFidelity)

Image quality measurements are a critical step when it comes to AR waveguide development and manufacturing. OptoFidelity's WG-IQ system (Figure 7) was used to quantify the image quality performance of the samples produced in this collaboration. Image quality measurements were used to assess overall manufacturing capabilities and provide feedback for process optimization. This included troubleshooting and refining steps across the production chain — ensuring that each stage meets the optical requirements for AR waveguides.

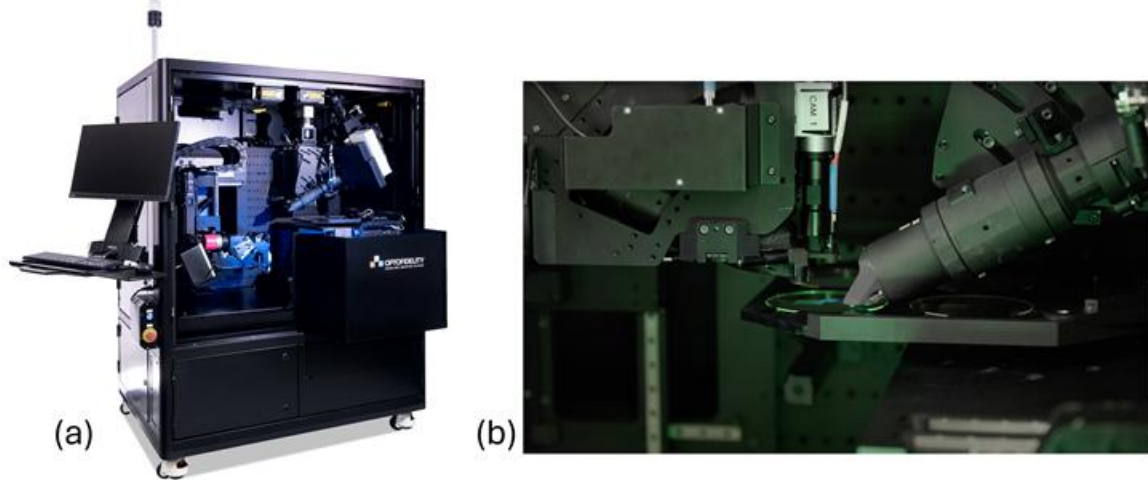

Figure 7 a) OptoFidelity WG-IQ. b) Projector (on the right) pupil matched to incoupler grating and camera (on the left) imaging at the eyebox.

WG-IQ system provides several configurable parameters that allow the measurement setup to be adapted to different waveguide designs and optical requirements. On the projector side, the exit pupil diameter is controlled using a motorized iris, the polarization state can be rotated continuously with a motorized polarizer, and the illumination wavelength can be selected between red, green, or blue light sources depending on the spectral band of interest.

On the imaging side, both the camera position and its optical parameters can be adjusted. The camera lens can be translated within the eyebox to probe performance at different pupil locations, and its entrance pupil size can be controlled with motorized iris to emulate different human-eye pupil diameters. The mechanical stages further support adjustments of wrap angle, and pantoscopic tilt to reproduce the intended operational geometry of the waveguide.

Positioning of the device under test (DUT) is fully automated. Confocal distance sensors and machine-vision alignment routines locate the waveguide surfaces, correct tip-tilt errors, and ensure precise translational placement between successive samples. This automation provides repeatable alignment and minimizes operator-dependent variability throughout the measurement process.

In this work, the WG-IQ system was configured with green, non-polarized illumination, a 3 mm projector exit pupil, and a camera pupil matched to this configuration. Waveguide efficiency, radiance non-uniformity, and MTF were used as the key metrics.

3. RESULTS

3.1 Grating tolerance study

Based on metrology data the following process-induced deviations were introduced successively into the nominal design model: (1) gaps between discretized grating regions, (2) variations in fill factor and grating depth, (3) deviations from the nominal 25° slant angle for the in- and out-coupling gratings, (4) sidewall tapering in the slanted grating profiles, and (5) edge rounding at the tops and bottoms of the grating ridges. See Figure 8.

The simulation results established a clear hierarchy of sensitivity to the characterized process variations. At the lowest level of impact, gaps between discretized grating regions at dimensions relevant to the mastering process exhibited negligible influence on optical performance. Far more consequential were deviations in grating height and fill factor, which caused pronounced degradation in efficiency. Similarly critical were deviations from the nominal 25° slant angle in the in- and out-coupling gratings. The most complex effect arose from sidewall tapering. Its initial inclusion appeared to increase efficiency relative to other non-ideal cases; however, a detailed analysis attributed this not to a beneficial impact of the tapered geometry itself, but to compensation effects from an associated, unintended increase in the local effective fill factor. Finally, edge rounding at the ridge tops and bottoms introduced a small but measurable secondary effect.

For the provided set of grating tolerances, a combined simulation predicted a worst-case total efficiency reduction for the waveguide of up to a factor of two relative to the ideal nominal design. This result quantifies the performance margin required for a robust process and establishes a clear optical benchmark for validating the R2P manufacturing line.

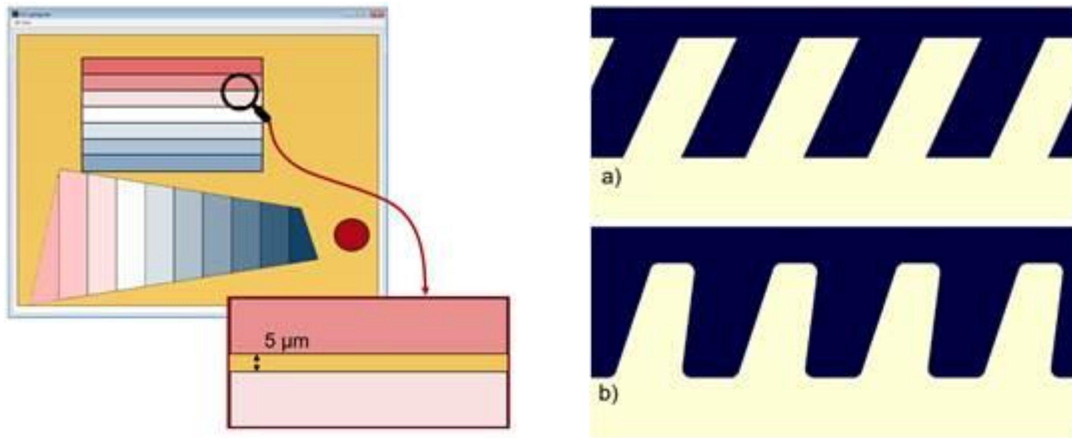

Figure 8 (left) Visualization of gaps between grating regions with different parameters, (right) Comparison of the cross section of an outcoupling grating region geometry for a) nominal design and b) including fabrication errors (2) - (5).

Overall, this tolerance study provides a crucial insight for high-precision manufacturing: transitioning from binary to slanted gratings significantly expands and tightens the critical parameter space. While fundamental parameters like fill factor and grating height remain essential to control, the introduction of a slant angle and the associated risk of profile tapering introduce additional, sensitive tolerance dimensions. This increased complexity makes the slanted-grating waveguide an ideal benchmark for validating a scalable process like R2P nanoimprint. The quantified sensitivity data

enable performance estimation from structural metrology and clearly define the tighter fabrication controls required to harness the full optical potential of next-generation AR waveguides.

3.2 Mastering

The ridge widths (measured at half depth) on the master for the IC, OC and EPE are within +/-0.4%, -3.6% to +6.5% and +1.5% to +2.4% of the target values, respectively. The etch-depth of the gratings on the master is pre-compensated to account for 6% material shrinkage from master to second generation working master that is used for the further replications. The measured grating depths on the master are within +/-1%, -5.2% to +2.3 and -0.4% to +4.5% of the target depths for IC, OC and EPE, respectively. The tapering angles of the slanted gratings are measured to deviate from the target angle of 24.9° by ±0.5° for IC and by 1.5° to 6.5° for OC.

3.3 Image quality

A total of 30 waveguide samples were evaluated using three image-quality metrics derived from WG-IQ measurements: efficiency, MTF50, and radiance non-uniformity. Efficiency was calculated as the average optical throughput across the full field of view. MTF50 was obtained by extracting the 50% contrast spatial frequency at nine field points across the waveguide's field of view and averaging the resulting values. Radiance non-uniformity was calculated from full-field illumination images by selecting multiple regions of interest and determining the non-uniformity as the difference between the maximum and minimum radiance values divided by the average radiance across all selected regions.

To allow comparison across the dataset, all metrics were standardized using Z-scores. The combined Z-score plot in Figure 1 provides an initial overview of sample-to-sample variability and highlights potential outliers within the production batch.

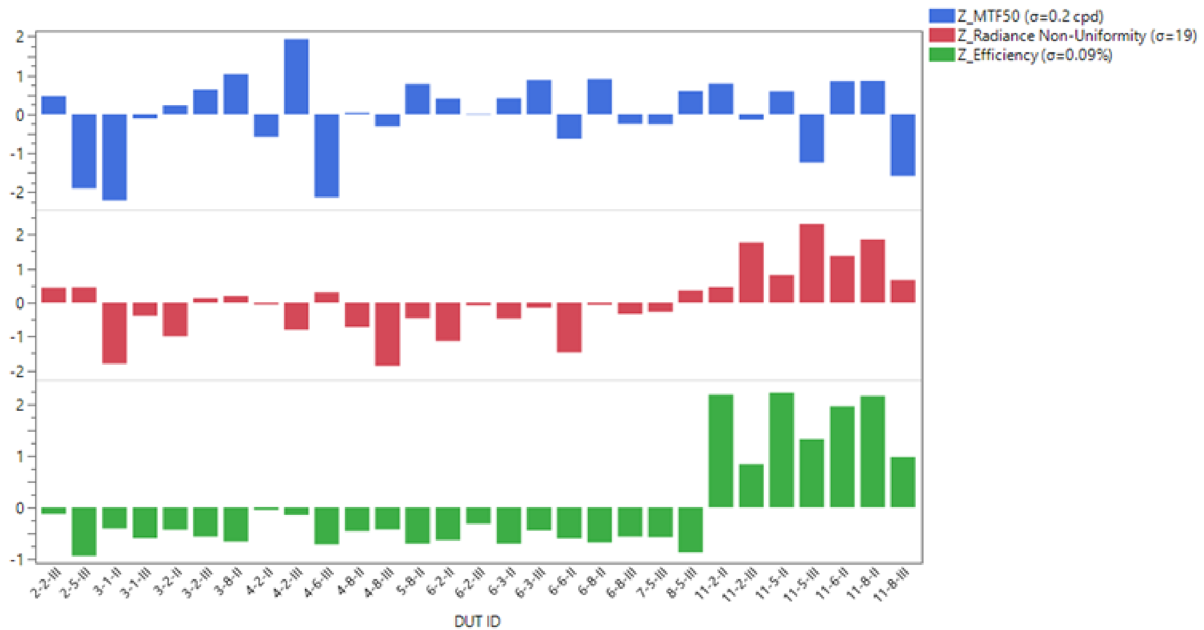

Figure 1 Z-score plots for efficiency, MTF50 and Radiance non-uniformity measurements.

The Z-score comparison of the 30 samples revealed distinct behaviors across the evaluated metrics. For MTF50, no clear trends were observed with respect to production cycle, or resin type. Interpreting the Z-score distribution is aided by the underlying standard deviation of the metric: the absolute variation in the dataset was 0.2 cycles per degree, indicating that even samples appearing as outliers in Z-score space differ only modestly in absolute terms. Efficiency showed a clear resin-dependent trend. Samples from production cycle 11, fabricated with PixNIL JCS1, showed efficiency values more than two standard deviations above the group mean. Given that the standard deviation for efficiency was 0.09%, this reflects a meaningful shift in performance relative to samples produced with PixNIL JT1. Within groups using the same

resin, no systematic trends were observed. Radiance non-uniformity demonstrated a similar resin-driven separation, but with opposite behavior: samples produced with PixNIL JCS1 showed higher non-uniformity than those produced with PixNIL JT1. Overall, the Z-score analysis indicates that the choice of resin has a significant impact on efficiency and radiance non-uniformity, while MTF50 remains unaffected.

Principal component analysis was performed on the Z-scored results and plotted in Figure 2. Component 1 accounts for 56.1% of the variance, while Component 2 accounts for 32.7%, for a combined total of 88.8%.. The score plot shows a clear separation by resin along Component 1: samples made with PixNIL JCS1 cluster at higher Component 1 score, whereas PixNIL JT1 samples cluster toward lower score. This indicates that resin choice is the dominant source of variation in the dataset.

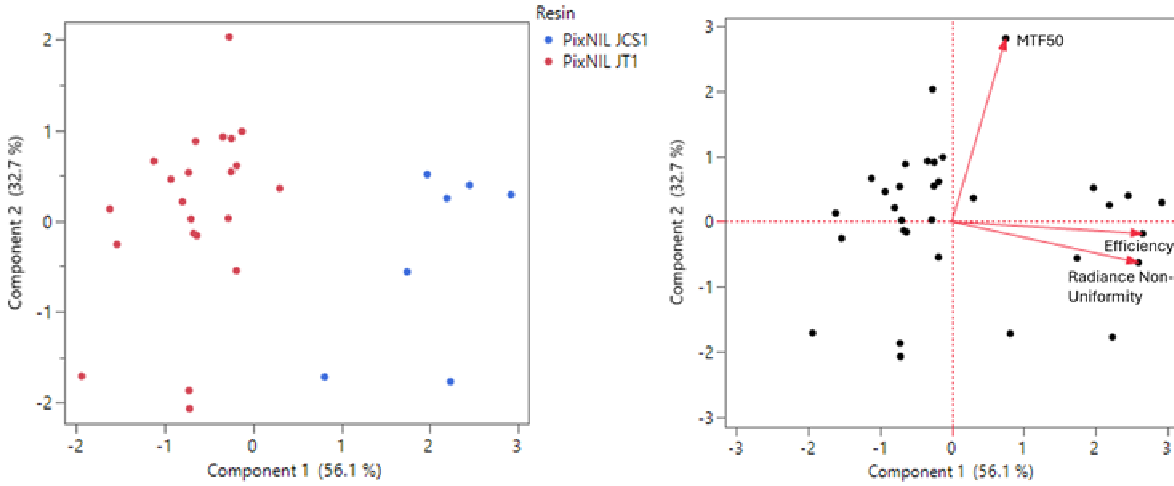

Figure 2 PCA of Z-scored WG-IQ metrics. Left: score plot colored by resin; the separation along Component 1 (56.1%) reflects a resin-driven trade-off between efficiency and radiance non-uniformity. Right: biplot showing efficiency and radiance non-uniformity aligned with Component 1 and MTF50 aligned with Component 2 (32.7%), indicating that resolution is largely independent of the resin-driven effects.

The biplot loadings indicate that efficiency and radiance non-uniformity are nearly colinear and aligned with Component 1, implying a strong positive correlation between these two metrics across samples. In practice, samples with higher efficiency also tend to exhibit higher non-uniformity, and vice versa. MTF50 loads primarily on Component 2 and is approximately orthogonal to the efficiency/non-uniformity direction, consistent with the Z-score analysis showing that MTF50 is largely independent of resin, wafer, or production cycle effects.

4. CONCLUSION

Based on the image quality measurements, resin choice was the main source of variation: PixNIL JCS1 samples showed higher efficiency but also higher radiance non-uniformity, while MTF50 remained stable across all samples. The principal component analysis confirmed these trends and indicated consistent manufacturing performance within each resin group.

Bridging metrology and simulations remained a central goal of this work, although complete integration was not fully achieved. In practice, the simulation model must replicate the metrology system closely enough to enable meaningful comparison, yet both domains involve inherent compromises. Metrology systems include optical and mechanical imperfections and alignment tolerances, while advanced simulation models can require substantial computational resources to generate equivalent datasets. Effective use of simulations therefore requires careful decisions about which system components to model accurately and which to approximate, and metrology must in turn provide data that is both relevant to the intended use case and compatible with the assumptions of the model. Addressing these challenges is an essential part of developing the kind of tightly integrated, high-throughput manufacturing workflows that will enable scalable production of high-quality AR waveguides for next-generation devices.

ACKNOWLEDGMENTS

The authors would like to thank their colleagues for their support on this work, with special thanks to Ievgen Kurylo, Lotje Jobse, Miloud Titou, Muhammad Ali and Rob Timmers from Morphotonics B.V. Funded by the European Union. Views and opinions expressed are however those of the author(s) only and do not necessarily reflect those of the European Union or European Innovation Council and SMEs Executive Agency (EISMEA). Neither the European Union nor the granting authority can be held responsible for them.

This manuscript was prepared with assistance from Microsoft Copilot to improve figures and linguistic readability.

REFERENCES

[1] M. Jotz et al., "The path towards mass manufacturing of optical waveguide combiners via large-area nano-imprinting," Proc. SPIE 11931, 1193109 (2022).
[2] S. Steiner et al., "Enabling the Metaverse through mass manufacturing of industry-standard optical waveguide combiners," Proc. SPIE 12449, 1244906 (2023).
[3] S. Steiner et al., "Exploring the boundaries of large-area nanoimprinting for mass production of AR waveguides" Proc. SPIE 12913, 129131D (2024).
[4] M. Jotz et al., "High strength laser cutting of high refractive index wafers for augmented reality" Proc. SPIE 12449, 124491U (2023).
[5] B. Bilenberg et al., "Integration of wafer and plate-based NIL for scalable manufacturing of high-quality AR waveguides" Proc. SPIE 13414, 1341418 (2025).
[6] E. Ercan et al., "Unlocking High-Throughput Low-Cost Fabrication of AR Waveguides via Cypris X600 Nanoimprint Platform" To be presented in the SPIE AR|VR|MR (2026).